REPORT DOCUMENTATION PAGE

AFRL-SR-BL-TR-01-

0611

1. AGENCY USE ONLY *(Leave blank)*	2. REPORT DATE	3. REPOR.
		01 FEB 99 - 30 NOV 99

4. TITLE AND SUBTITLE
Global/Local Design Optimization of A Power Distribution System

5. FUNDING NUMBERS
F49620-99-1-0104

6. AUTHOR(S)
Zafer Gurdal

7. PERFORMING ORGANIZATION NAME(S) AND ADDRESS(ES)
Engineering Science and Mechanics Department - 0219
Virginia Tech
Blacksburg, VA 24061

8. PERFORMING ORGANIZATION REPORT NUMBER

9. SPONSORING/MONITORING AGENCY NAME(S) AND ADDRESS(ES)
AFOSR/NM
801 N. Randolph Street Room 732
Arlington, VA 22203-1977

10. SPONSORING/MONITORING AGENCY REPORT NUMBER
F49620-99-1-0104

11. SUPPLEMENTARY NOTES

12a. DISTRIBUTION AVAILABILITY STATEMENT
APPROVED FOR PUBLIC RELEASE, DISTRIBUTION UNLIMITED

12b. DISTRIBUTION CODE

13. ABSTRACT *(Maximum 200 words)*

A mathematical optimization technique is used to design several components of a power distribution system for next generation aircraft. A simple interconnected system consisting of an input filter and a DC-Dc buck converter is used as the prototype for the optimization demonstration. The components are designed for minimum weight subject to performance, stability, and peak voltage constraints. Optimized designs for each of the individual subsystems and for the integrated system are presented. It is shown that there is interaction between the filter design problem and the converter design problem, and that weight improvements can be obtained by taking these interactions into account. The automated design scheme described enables designers to obtain optimized subsystem designs in a time efficient manner.

20011212 104

14. SUBJECT TERMS	15. NUMBER OF PAGES
	26
	16. PRICE CODE

17. SECURITY CLASSIFICATION OF REPORT	18. SECURITY CLASSIFICATION OF THIS PAGE	19. SECURITY CLASSIFICATION OF ABSTRACT	20. LIMITATION OF ABSTRACT

Global/Local Design Optimization of A Power Distribution System

Final Report

Sponsored By

Air Force Office of Scientific Research

AFOSR Contract Number: F49620-99-1-0104

Dr. Neal D. Glassman, Program Manager
AFOSR/NM
801 North Randolph Street, Room 732
Arlington, VA 22203-1977

March 31, 2000

Prepared by

Zafer Gürdal, Scott Ragon

Engineering Science and Mechanics Department - 0219

Douglas Lindner

Bradley Department of Electrical and Computer Engineering - 0111

Virginia Tech

Blacksburg, VA 24061

Objectives

Assist in the development of optimization methodologies for the design of next generation power systems. Implement a global/local optimization technique to achieve a cost effective design optimization tool.

Status of the Effort

A mathematical formulation for the definition of the optimization problem for automated design optimization of power circuits with regenerative power was completed.

Accomplishments/New Findings

1. A well-posed optimization problem was formulated for the design of a filter. It was shown that the design cycle of the filter was significantly reduced. This formulation is expected to significantly impact the industrial design of filters.

2. A well-posed optimization problem was formulated for the design of a dc-to-dc power converter.

3. The design of a converter plus filter was accomplished using the optimization formulations of the two subsystems developed above. It is shown that the joint optimization is preferable to optimization of the components separately.

4. A preliminary plan for applying global/local design methodologies to the power system design problem was formulated.

Personnel Supported

Dr. Scott Ragon was supported part time as a Postdoctoral Research Associate.

Publications

The following paper is under review for a journal publication:

Ragon, S. A., S. Chandrasekaran, Z. Gürdal, and D. K. Lindner, "Optimal Design of a Power Distribution System," submitted for publication, AIAA Journal of Aircraft, March 2000.

The following conference papers have been presented:

Ragon, S. A., S. Chandrasekaran, Z. Gürdal, and D. K. Lindner, "Optimal Design of a Power Distribution System," accepted for the 38th AIAA Aerospace Sciences Meeting and Exhibit: Multidisciplinary Design Optimization, Reno, NV, Jan 10 - 13, 2000.

Chandrasekaran, S., K. Louganski, D. K. Lindner, S. Ragon, and Z. Gürdal, "Optimized Design of Power Distribution Systems foe Next Generation Aircraft," *Proceedings of the 17 Annual Power Electronics Seminar*, Blacksburg, VA, Sept. 19 - 21, 1999, pp.200-206.

Interactions/Transitions

Lockheed Martin: Catherine Frederick and Gordon Lu.

Schneider Electric of France funded a project to extend the design optimization capabilities to cost optimization of power circuits.

New Discoveries, Inventions, or Patent Disclosures

There were no new disclosures during this period.

Honors/Awards

No honors or awards were accepted during this period.

This research project was performed in conjunction and cooperation with an existing research program entitled "Subsystem Integration for Efficient Power Flow In 21st Century Airlifters''. This existing program is sponsored by the Air Force Office of Scientific Research under the New World Vistas Program (AFOSR Grant Number: F49620-97-1- 0254). This "parent research" program has as its primary goal the simulation and design of power distribution systems for the next generation transport aircraft. One of the principal investigators of this project, Dr. Lindner, is also a principal investigator for the parent research project.

OPTIMAL DESIGN OF A POWER DISTRIBUTION SUBSYSTEM

S.A. Ragon,* S. Chandrasekaran,† D.K. Lindner,† Z. Gürdal,* and D. Boroyevich†
*Department of Engineering Science and Mechanics
†Bradley Department of Electrical and Computer Engineering
Virginia Polytechnic Institute and State University
Blacksburg, VA 24061

ABSTRACT

A mathematical optimization technique is used to design several components of a power distribution system for next generation aircraft. A simple interconnected system consisting of an input filter and a DC-DC buck converter is used as the prototype for the optimization demonstration. The components are designed for minimum weight subject to performance, stability, and peak voltage constraints. Optimized designs for each of the individual subsystems and for the integrated system are presented. It is shown that there is interaction between the filter design problem and the converter design problem, and that weight improvements can be obtained by taking these interactions into account. The automated design scheme described enables designers to obtain optimized subsystem designs in a time efficient manner.

1. INTRODUCTION

In the next generation transport aircraft, it is projected that all power will be distributed and processed electrically. Electrical power will be utilized for driving a diverse array of aircraft subsystems that are currently powered by hydraulic, pneumatic, or mechanical means. These subsystems include flight control actuation systems, environmental control systems, and several other utility subsystems. The power distribution system therefore plays a central role in the developing concepts of next generation aircraft. The principal objective of this research effort is to develop and demonstrate optimization methods that facilitate the design of these power distribution systems.

The current primary interest is in next generation power distribution systems built around a 270V DC distribution bus. This bus is regulated by switching power converters. Most of the loads, including the actuators, are also regulated using switching power converters. Other devices in the power system are filters and relays that serve to control the interaction of the various components of the power system.

The design of these power systems presents challenges on several different levels. The design of the components themselves is quite complex, particularly the switching power converters. When these converters are interconnected into a system, additional design considerations arise. For example, this type of power distribution system allows for power flow in both the forward direction from the generator to the loads and in the reverse direction from the loads to other loads and the generator. In other words, the system is capable of generating power, for example, upon reversal of the control surfaces,and possesses the property of having *regenerative power flow* that needs to be dealth with. The results reported in this paper address two consequences of this regenerative power flow. First, the regenerative power flow will cause voltage peaks on the bus. Therefore, the individual component design must take into account these system level transient

phenomena. Second, the presence of regenerative power flow indicates tight coupling between the individual power system components. Therefore, the stability of the global system must be insured from the local component design.

Mathematical optimization techniques have found abundant application for the design of high performance converter and drive systems [1-3]. However, optimization methods for the design of aircraft or shipboard power distribution systems where efficiency, size, and weight are of paramount importance have received very little attention in the past [4]. The design of these power distribution systems is extremely involved due to the preponderance of power converters, advanced motor drives, and actuation systems. In addition, any design methodology must take into account the complex interactions between different subsystems.

In the following we develop an optimization procedure to facilitate the design of a power system. The proposed optimization procedure is demonstrated on a simple interconnected system (henceforth referred to as the sample system) consisting of a regulated DC-DC buck converter preceded by an input filter. The sample system, although not as complicated as a typical aircraft power system, captures the essential features of the optimization procedure. The procedure is formulated to yield realistic designs for each component. Then, the procedure is extended to the sample system to address system wide design considerations. In order to assess the validity of the results obtained from the optimizer, the optimal designs are compared to a filter built for a three-phase buck converter for a telecommunications application [5].

The sample system is introduced in section 2. The optimized design of the input filter as an independent subsystem is presented in section 3, and, this optimal design is compared to a nominal design to illustrate the effectiveness and efficiency of the proposed methodology. The optimized design of the converter as an independent subsystem is then presented in section 4 following a methodology similar to that used for the input filter. In order to evaluate the effects of system interaction on the optimal design process, the filter and converter were combined to form an interconnected system and optimized simultaneously. These results are presented in section 5.

2. SAMPLE SYSTEM

In this paper we will demonstrate the optimization procedure on a sample system that captures the salient features of the optimization. The sample system consists of an input filter followed by a regulated DC-DC buck converter is shown in Figure 1.

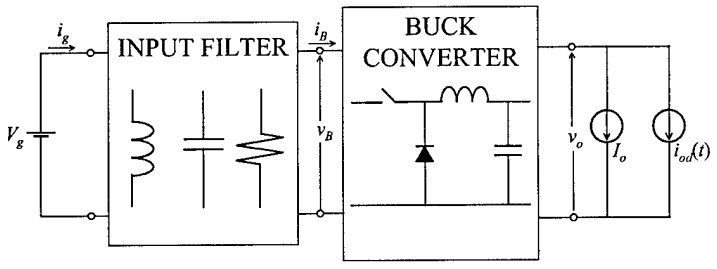

Figure 1. Block diagram of the sample system.

The power is supplied by the aircraft power bus, which is assumed to be a stiff DC source of $V_g = 270\text{V}$. The buck converter is representative of motor drives commonly found in aircraft

power systems. The converter is loaded by a fixed DC current source I_o (to represent the average power drawn).

Switching converters, due to their high frequency switching behavior, inject an appreciable amount of high frequency noise into the system. This high frequency noise results in what is known as Electromagnetic Interference (EMI) between the converter and other interconnected systems. Input filters are added at the front end of these converters in order to prevent the switching noise from entering the source subsystem. Stringent EMI specifications exist that impose upper bounds on the input filter transfer characteristics at different frequency ranges as dictated by the specific application.

A distinguishing feature of the modern aircraft power distribution systems is the regeneration of energy from the flight control actuators to the DC bus during certain operating regimes. The regenerative flow of power occurs as a transient disturbance on the DC bus and results in intolerably large voltage swings on the same. To account for the effect of regenerative power flow, the load disturbance $i_{od}(t)$ indicated in Figure 1, is represented by a pulse load with duration T_p as shown in Figure 2.

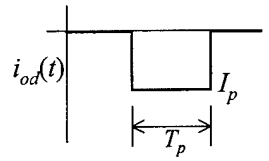

Figure 2. Load disturbance profile

The nominal operating conditions for the sample system are given below in Table 1.

Table 1. Nominal Operating Conditions for Sample System

Variable	Description	Value
V_g	Filter input voltage	*270V*
V_B	Filter output voltage	*270V*
V_o	Converter output voltage	*100V*
D	Converter duty cycle	*Vo/Vg*
I_o	Converter average load current	*15A*
I_B	Converter input current	$I_o(V_o/V_g)$
I_p	Peak value of pulse disturbance	*-20A*
T_p	Duration of pulse disturbance	*10ms*

The goal of the optimization is to design these two subsystems such that: 1) each subsystem meets its own performance specifications (to be described below), 2) the overall system is stable within prescribed stability bounds, 3) the effect of the transient disturbance source $i_{od}(t)$ at the output of the buck converter on the input voltage of the converter is limited, and 4) the overall weight of the system is minimized.

In the sections that follow, we will discuss the optimization of each subsystem separately, and then the joint optimization of the whole system.

3. OPTIMIZED DESIGN OF INPUT FILTER

In this section we will discuss the optimal design of the input filter shown in Figure 3. This topology was used for a three-phase buck rectifier for a telecommunications application [5].

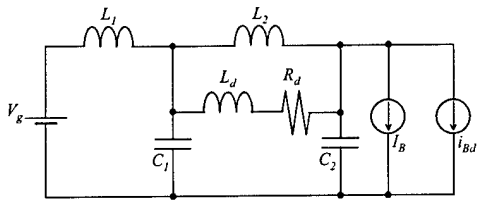

Figure 3. Schematic of input filter used in sample system.

To formulate the optimization procedure it is necessary to: 1) develop the model of the filter, 2) identify the design variables, 3) specify the constraints, and 4) define the objective function.

Input Filter Model

The model for this subsystem can easily be developed using network analysis. For the optimization procedure, the model is written in the standard state space form

$$\dot{x} = Ax + Bu \tag{1}$$

$y = Cx + Du$, where

$x = \begin{bmatrix} i_{L1} & i_{L2} & i_{Ld} & v_{C1} & v_{C2} \end{bmatrix}^T, u = \begin{bmatrix} v_g & i_B \end{bmatrix}^T$

$y = \begin{bmatrix} v_B & i_g \end{bmatrix}^T$

Design Variables

Design variables for the input filter shown in Figure 3 include the capacitance values C_1 and C_2, and resistance value R_d. In addition, we must design the three inductors. In the present work the inductor design includes the physical design of the inductor's components, not just the selection of the value of the inductance, L. The inductors are assumed to be typical EE cores as shown in Figure 4.

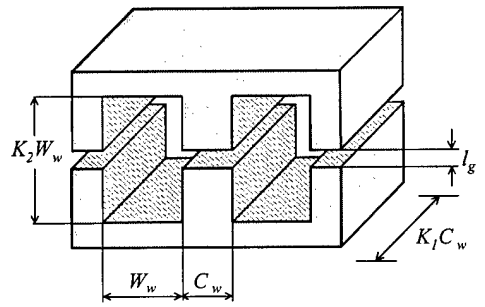

Figure 4. EE Core and its relevant dimensions

The quantities K_1 and K_2 shown in Figure 4 are assumed to be fixed and represent the aspect ratios of the center leg and the window, respectively. The other physical variables governing the

design of each inductor are listed in Table 2. Note that these variables include parameters related to the windings and wire size.

Table 2. Physical variables associated with inductor design

Variable name	Description
n	Number of turns
A_{cp}	CSA of winding
C_w	Center leg width
W_w	Window width
l_g	Airgap length

The inductance as a function of these physical variables is given by $L = \frac{\mu_o K_1 C_w^2 n^2}{l_g}$. The complete set of input filter design variables is listed in Table 3.

Table 3. Design Variables for the Input Filter

Design Variable	Description
C_1	Filter capacitance
C_2	Filter capacitance
R_d	Filter resistance
N_d	Number of turns for L_d
A_{cpd}	CSA of winding for L_d
C_{wd}	Center leg width for L_d
W_{wd}	Window width for L_d
l_{gd}	Airgap length for L_d
N_1	Number of turns for L_1
A_{cp1}	CSA of winding for L_1
C_{w1}	Center leg width for L_1
W_{w1}	Window width for L_1
l_{g1}	Airgap length for L_1
N_2	Number of turns for L_2
A_{cp2}	CSA of winding for L_2
C_{w2}	Center leg width for L_2
W_{w2}	Window width for L_2
l_{g2}	Airgap length for L_2

Constraints

The input filter design constraints are subdivided into physical, performance, and stability constraints as explained in the following subsections.

Physical Constraints: These constraints are defined to guarantee physically meaningful dimensions for the core and windings used in the inductor (Figure 4). They are defined as follows [2]:

- The widths of the center leg C_w, and of the window W_w are not allowed to be less that 1mm.
- In order to ensure sufficient mechanical strength for the winding, the copper wire used cannot be greater than 30AWG, which is equivalent to a cross-sectional area of 7.29 x 10-8 m2.
- The number of turns in the inductor cannot be less than one.

- The current density in the windings of the inductor cannot be greater than maximum allowable current density for copper.
- The available window area of the EE core must be large enough to accommodate the windings of the inductor, see Equation 2 (see Table 2 for inductor variables).

$$K_2 W_w^2 > \left(\frac{nA_{cp}}{F_w} + W_{bob} K_2 W_w \right) \text{where,}$$

F_w, window fill factor = 0.4

W_{bob}, bobbin thickness = 1.5mm

K_2, Window area aspect ratio = 3 (2)

- The dimensions of the inductor should be such that the maximum allowable saturation flux density for core material (which is assumed to be ferrite) is not exceeded, Equation 3.

$$B_{sp} > \frac{LI_{L(pk)}}{nK_1 C_w^2}, \quad (3)$$

B_{sp}, saturation flux density of ferrite = 0.3T

K_1, center leg aspect ratio = 1.5

Performance Constraints: Performance constraints are further classified as frequency domain and time domain constraints:

Frequency domain constraints: As mentioned earlier, input filters are added at the front end of switching converters in order to prevent the high frequency noise from entering the source subsystem. Stringent EMI specifications exist that impose upper bounds on the input filter transfer characteristics at different frequency ranges as dictated by the specific application.

The EMI specifications on the input filter are typically translated into frequency domain constraints on the input-output transfer function of the input filter

$$\frac{V_B(j\omega)}{V_g(j\omega)} = A_v(j\omega) \quad (4)$$

The frequency response function for a typical input filter is shown in Figure 5.

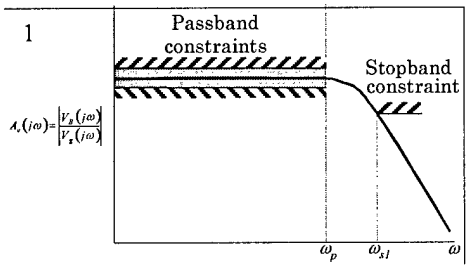

Figure 5. Definition of frequency domain performance specifications for the input filter

Two types of constraints exit for the frequency response function: low frequency constraints and high frequency constraints. The transfer of power from the source to the load occurs almost entirely in the low frequency region. Hence, in order to achieve a low pass filter characteristic, the frequency response function must be near unity in the passband. These transmission requirements are defined in terms of upper and lower bounds on the input-output transfer function of the filter up to a passband frequency, ω_p, as shown in Figure 8. For the present problem, the passband constraint is defined as :

$$-1\,dB \le |A_v(j\omega)| \le 6\,dB \text{ for } 0 \le \omega \le 2\pi 5\times 10^3\, rad/s. \tag{5}$$

The frequency boundaries for the stopband and passband constraints were chosen based on the assumption that the converter to which the filter is attached has a nominal switching frequency of 100 kHz. This high frequency switching generates a high frequency ripple that must be attenuated. Hence, the frequency response function in the stopband must be small. For the present problem, a stopband constraint was imposed above the frequency, ω_{sl}, as (see Figure 5):

$$|A_v(j\omega)| < -60\,dB \quad \text{for } \omega > 2\pi \cdot 50\times 10^3\, rad/\sec. \tag{6}$$

Time Domain Constraints: In the sample system shown in Figure 1, a disturbance current load at the output of the buck converter develops transient voltage swing at the output of the input filter. To capture this disturbance in the filter problem, the input filter is terminated by two current sources: I_B that represents the DC current drawn by the converter, and $i_{Bd}(t)$ that represents the transient load disturbance (Figure 3). A time domain constraint, which imposes an upper bound on the maximum transient excursion of the output voltage of the filter, is imposed as indicated in Figure 6 to limit the disturbance. For the present work, the maximum transient voltage excursion limit was 20 V:

$$\Delta v_B < 20\ V. \tag{7}$$

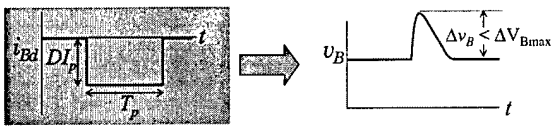

Figure 6. Time domain constraint for input filter

Stability Constraints

Because the input filter consists only of passive components it is generally internally stable (with all its eigenvalues in the left half of the s-plane). However, the input filter is notorious for causing instability due to its interaction with a regulated converter. It can be shown that a regulated power converter can have negative input impedance that, due to the addition of a front-end input filter, might cause the interconnected system to become unstable. Constraints that guarantee stability of the interconnected system are defined in the frequency domain using the Middlebrook impedance ratio criterion [7]. The impedance ratio criterion is explained in the following.

A generic subsystem interface is shown in Figure 7. The interconnected subsystems are, in general, nonlinear and are represented by average models that are linearized about an operating point. The current i_I, and voltage v_I, at the interface are given by Equation 8.

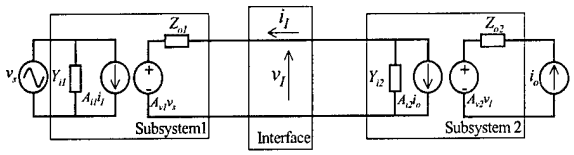

Figure 7. Generic Subsystem Interface

$$\begin{aligned} i_I &= A_{i2} i_o + Y_{i2} v_I \\ v_I &= A_{v1} v_s - Z_{o1} i_I . \end{aligned} \tag{8}$$

The sufficient condition for the stability of the interconnected system is given by:

$$\begin{aligned} &\left\| Z_{o1}(j\omega) \right\| \cdot \left\| Y_{i2}(j\omega) \right\| \ll 1 \\ &\Rightarrow \left\| Z_{o1}(j\omega) \right\| \ll \frac{1}{\left\| Y_{i2}(j\omega) \right\|} . \end{aligned} \tag{9}$$

Equation (9) is traditionally known as the Impedance Ratio Criterion. The stability constraint for the input filter is, therefore, specified in terms of these terminal impedances. The input filter schematic showing only the relevant impedances is shown in Figure 8.

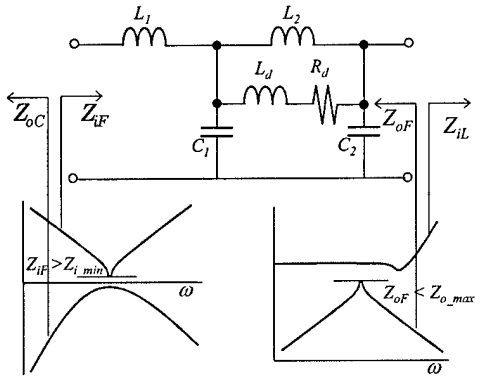

Figure 8. Impedances at the terminals of the input filter.

The impedance looking out of the output terminals of the filter is designated Z_{iL} and is the input impedance of the buck converter. The impedance looking out of the input terminals is designated Z_{oC} and is the output impedance of the source subsystem (which, in this case, is represented by an ideal voltage source). Since the impedances Z_{oC} and Z_{iL} are given, upper (Z_{o_max}) and lower (Z_{i_min}) bounds on the output and input impedance of the filter, respectively, are specified to ensure sufficient separation between them and the impedances of the source and load subsystems:

$$\begin{aligned} Z_{i\_min} &= \min_{\omega} \left(\left| Z_{iF}(j\omega) \right| \right) > 3 \text{ dB} \\ Z_{o\_max} &= \max_{\omega} \left(\left| Z_{oF}(j\omega) \right| \right) < 15 \text{ dB}. \end{aligned} \tag{10}$$

Objective Function

The objective function is the weight of the input filter. The total filter weight is the sum of the weights of the inductors, capacitors, and resistors:

$$J = W_L + W_C + W_R \tag{11}$$

The weight of an inductor is determined as the sum of the weights of iron and copper used in the core and windings, respectively

$$W_L = W_{fe} + W_{cu} \tag{12}$$

The weight of the copper is given by:

$$\begin{aligned} W_{cu} &= D_{cu} Vol_{cu}, \text{ where } D_{cu} = 8900\text{kg/m}^3 \\ Vol_{cu} &= MLT \cdot n \cdot A_{cp}, \text{ where} \\ MLT &= 2F_c C_w (1 + K_1), \text{mean length/turn} \end{aligned} \tag{13}$$

The weight of the iron used in the EE core is given by:

$$\begin{aligned} W_{fe} &= D_{fe} Vol_{fe}, \text{ where } D_{fe} = 7800\text{kg/m}^3 \\ Vol_{fe} &= Z_p A_p, \text{ where} \\ Z_p &= 2(1 + K_2) W_w + \frac{\pi}{2} C_w, \text{ magnetic path length} \\ A_p &= K_1 C_w^2, \text{ Area of crosssection of center leg} \end{aligned} \tag{14}$$

The weight of a capacitor is approximated as a function of the energy stored in it and is given by following equation, where the constant α_C was obtained from manufacturer data sheets:

$$W_C = \alpha_C C V_C^2 \tag{15}$$

Finally, the weight of the resistor is approximated as a function of the energy dissipated in it.

$$W_R = \int_0^t R \cdot i_R^2 \cdot \mathrm{dt} \tag{16}$$

Optimization Results

Optimization was performed using the VisualDOC optimization software [8] using the Modified Method of Feasible Directions algorithm [9]. The transient peak voltage constraint was enforced by imposing an upper bound constraint on the maximum output voltage obtained from a time domain simulation of the filter response. Constraint derivatives were computed using finite differences. Depending on the initial design used to start the optimization iterations, convergence was obtained within approximately 200 function evaluations (here a single function evaluation

includes both a time domain simulation and frequency domain computations). The optimizations were achieved in approximately 40 minutes on a 500 MHz Pentium III PC.

In order to assess the validity of the results obtained from the optimizer, the optimal designs were compared to a filter built for a three-phase buck converter for a telecommunications application [5]. This hardware design, developed without the use of the optimizer, is referred to here as the nominal design.

The optimization algorithm used for the present work belongs to a class of optimization algorithms termed "gradient based methods". In order to begin the optimization process, these algorithms are typically provided with an initial design. Once an initial design is specified, gradients of the objective function and constraints are computed with respect to the design variables to compute a search direction in the design space. Next, the design space is searched along the computed direction so as to minimize the objective function while satisfying all the constraints. Gradients are then recomputed at the new design point, and the process continues until no further improvements are possible. If the design space contains several local minima, there is a possibility that a gradient based optimizer may be trapped by a local minimum, and the answer will depend on the selection of the initial design point. In order to increase the probability of finding the point with the smallest objective function value (the global minimum), it is customary to execute the optimization algorithm starting from several different initial designs. In the present work, it was found that there were local minima in the design space, although in all cases studied, even the local minima were lighter than the nominal design. The results reported here correspond to the best designs found during the course of the study.

The nominal and optimum design variables and the objective function are given in Table 4. The inductor values for the nominal and optimal designs based on the physical variables are provided in Table 5. Response quantities of interest for the nominal and optimal designs are given in Table 6. Response quantities that are at their upper or lower bounds are listed in bold face type. All the physical constraints on the inductor designs were active for the optimal design. The other active constraints for the optimized design were the lower bound constraint on the input impedance Z_{iF} and the stop-band constraint on the input-output transfer function. Note that the peak voltage constraint was violated for the nominal design.

Table 4. Optimization Results for Input Filter

Variable	Nominal value	Optimal value
n_1	29.53	19.94
A_{cp1}	0.630×10^{-5} m^2	0.530×10^{-5} m^2
C_{w1}	0.751×10^{-2} m	0.484×10^{-2} m
W_{w1}	0.682×10^{-2} m	1.017×10^{-2} m
l_{g1}	1.16×10^{-3} m	0.664×10^{-3} m
n_2	45.98	42.77
A_{cp2}	0.448×10^{-5} m^2	0.382×10^{-5} m^2
C_{w2}	0.985×10^{-2} m	0.939×10^{-2} m
W_{w2}	1.33×10^{-2} m	1.244×10^{-2} m
l_{g2}	1.29×10^{-3} m	1.03×10^{-3} m
n_d	16.06	7.79
A_{cpd}	0.349×10^{-5} m^2	0.359×10^{-5} m^2
C_{wd}	0.396×10^{-2} m	0.585×10^{-2} m
W_{wd}	0.978×10^{-2} m	0.564×10^{-2} m

l_{gd}	0.355 x 10^{-3} m	0.176 x 10^{-3} m
C_1	5 μF	7.19 μF
C_2	18.8 μF	27.70 μF
R_d	3 Ω	2.23 Ω
Weight	0.5279 kg	0.3692 kg

Table 5. Nominal and Optimal Inductor values

Variable	Nominal value	Optimal value
L_1	80 μH	26.49 μH
L_2	300 μH	296.77 μH
L_d	21.5 μH	22.29 μH

In order to compare the optimization results with the hardware (nominal) design, several additional optimization runs were performed corresponding to different values of the lower bound constraint Z_{i_min} on the input impedance. The resulting family of optimal designs is compared to the nominal design in Figure 9. For the same value (3.8 dB) of Z_{i_min}, the optimal design is 25% lighter than the nominal design. For the same weight, on the other hand, the minimum input impedance for the optimized design is approximately 47% higher than for the nominal design.

Table 6. Response quantities for nominal and optimal designs of input filter

Response variable	Nominal	Optimal
Minimum input impedance	3.81* dB	**2.99 dB**
Maximum output impedance	15.39 dB	9.11 dB
Passband maximum	5.63 dB	3.18 dB
Passband minimum	6.55 x 10^{-6} dB	7.94390 x 10^{-6} dB
Stopband maximum	-63.13dB	**-60.00 dB**
Peak output voltage	21.97* V	13.75 dB

*violated constraint

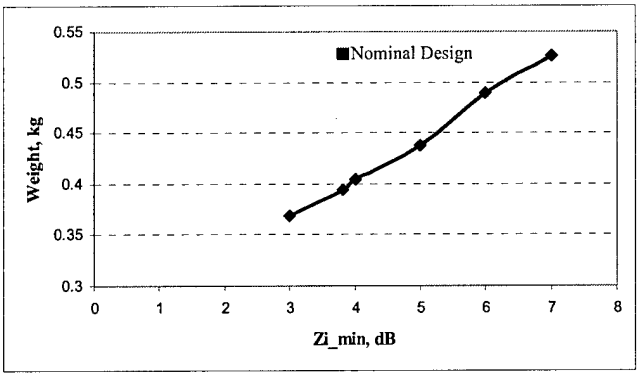

Figure 9. Weight of optimal designs as a function of the lower bound on the input impedance

In addition to providing weight savings in comparison to the nominal design, the optimal design methodology is automated and can considerably reduce design cycle time. Such an automated filter design tool may enable engineers with little experience in filter design to generate high quality filter designs in a short period of time.

4. OPTIMIZED DESIGN OF BUCK CONVERTER

Buck Converter Model

The schematic of the DC-DC buck converter is shown in Figure 10a. The switch-diode combination highlighted in Figure 10a is replaced by a single-pole double throw switch, known as the PWM switch, as shown in Figure 10b. The switch S is turned on (switch at position *a* in Figure 10b) and off (switch at position *b* in Figure 10b) at a fixed frequency to transform the input voltage v_g to a periodic square wave voltage v_L. The voltage v_L is then filtered by the *L-C* filter to obtain the output voltage v_o. The average value of the output voltage is varied by modulating the time interval the switch *S* is kept on.

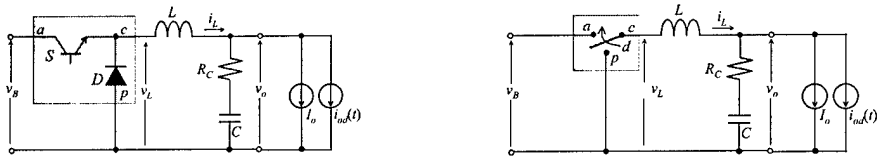

(a) (b)

Figure 10. Schematic of DC-DC Buck converter
(a) Realization with transistor-diode combination
(b) Realization with PWM switch

The fraction of the time period *T* for which the switch is kept on is known as the duty cycle *d* of the switch. The values of *L* and *C* and the switching frequency f_s, determine the switching ripple in the inductor current i_L, and output voltage v_o. In order to tightly regulate the average value of the output voltage to a fixed reference, a feedback compensator is used to control the duty cycle *d* of the switch against disturbances in the load current i_o, and input voltage v_B. Approximate waveforms of the inductor current and the output voltage including the switching ripple are shown in Figure 11.

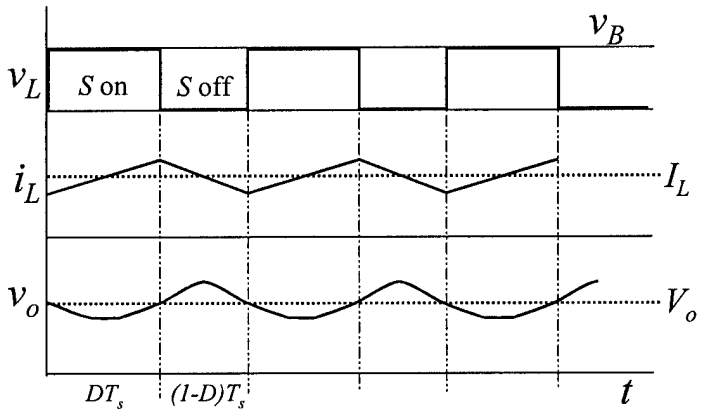

Figure 11. Switching waveforms of inductor current and output voltage

In this paper, an average model of the buck converter, which neglects the switching ripple in the currents and voltages, is used [6]. The average model of the buck converter replaces the switch-diode combination in the switch model (Figure 10a) by controlled current and voltage sources. A

multi-loop controller consisting of an inner inductor current loop and an outer voltage loop is used for the regulation of the output voltage to a fixed reference. Since average models of the converters are in general nonlinear, small signal models linearized around an operating point are derived. These linearized models are then used for the design of the current and voltage controllers. As already mentioned, the input voltage v_B, is represented by an ideal voltage source of 270V. The average model of the buck converter along with a block diagram of the controller is shown in Figure 12.

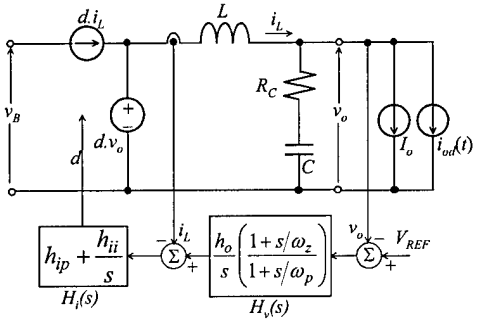

Figure 12. Average model of buck converter with inductor current and output voltage compensators

Design Variables

Design variables for the buck converter include the physical parameters governing the design of the inductor, capacitance C, the switching frequency of the converter f_s, and a set of parameters governing the feedback controller (h_o, ω_z, ω_p, h_{ip}, and h_{ii}). As with the filter, it is assumed that an EE core is used for the inductor (Figure 4). Table 7 contains a list of all design variables used for the buck converter.

Constraints

The performance, stability and physical constraints on the design of the buck converter are described in the following paragraphs.

Table 7. Design Variables for buck converter

Design Variable	Description
C	Capacitance
n	Number of turns for L
A_{cp}	CSA of winding for L
C_w	Center leg width for L
W_w	Window width for L
l_g	Airgap length for L
f_s	Switching frequency of buck converter
h_o	Voltage controller gain
ω_z	Voltage controller zero
ω_p	Voltage controller pole
h_{ip}	Current controller proportional gain
h_{ii}	Current controller integral gain

Performance Constraints

Frequency Domain Constraints: Two frequency domain constraints are imposed on the buck converter. These constraints can be explained with the help of the simplified block diagram of the closed loop buck converter shown in Figure 13. Frequency domain constraints for the buck converter are imposed as upper bounds on the maximum magnitude of the transfer function between the input and output voltage and the voltage loop gain crossover frequency.

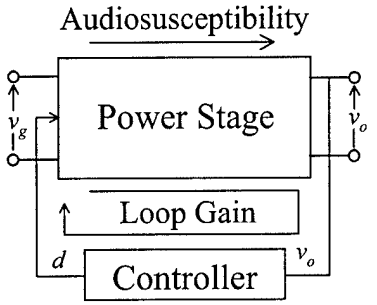

Figure 13. Simplified block diagram of closed loop buck converter

The transfer function between the input voltage v_g and the output voltage v_o is called the audiosusceptibility of the converter. A typical transfer function is shown in Figure 14a. An upper bound is imposed on this transfer function in order to guarantee sufficient rejection of any audio frequency disturbance introduced at the input voltage. This constraint can be stated as,

$$A_v = \max_{\omega} \left| \frac{V_o(j\omega)}{V_g(j\omega)} \right| < -30\,\text{dB} \tag{17}$$

The second constraint is imposed on the loop gain. The loop gain is the transfer function between the output voltage error V_{ref} - v_o, and the output voltage v_o. The characteristics of the loop gain transfer function determine the bandwidth and the stability margins of the closed loop system. A typical curve is shown in Figure 14b.

An upper bound constraint is also imposed on the crossover frequency of the voltage loop gain, ω_{cg}. This constraint is imposed for the following reasons:

1) Because the average model neglects the switching frequency ripple it is valid only for frequencies much lower than half the switching frequency. If a limit is not imposed on the crossover frequency ω_{cg}, a controller design could potentially be achieved with a bandwidth comparable to the switching frequency, which would render the model invalid.

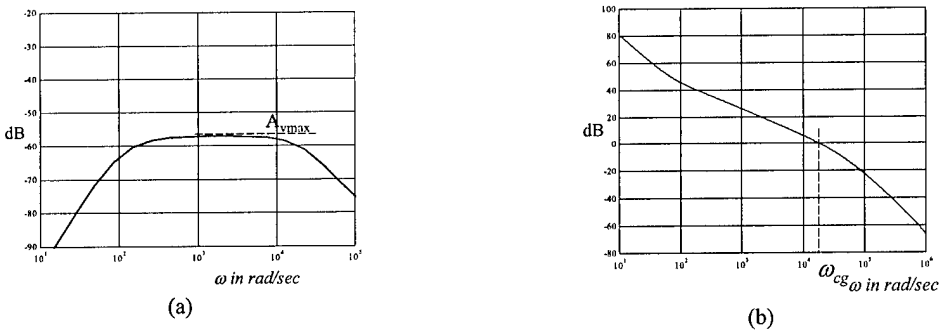

Figure 14. Frequency Domain Constraints for the buck converter (a) Audiosusceptibility, (b) Voltage loop gain

2) In order to attenuate the measurement noise, the loop gain must be low at high frequencies.

$$\omega_{cg} < \frac{2\pi f_s}{5} \tag{18}$$

Time Domain Constraints: As in the case of the input filter, time domain constraints are introduced to account for transient disturbances in the system. A pulse load disturbance represents the transient disturbance at the output of the buck converter. For the optimized design of the buck converter, a fixed resistance is included in series with an ideal voltage source as shown in Figure 15.

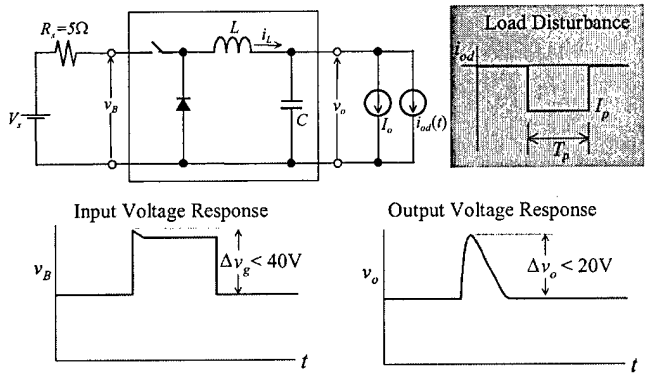

Figure 15. Time domain constraints for the converter

This fixed resistance was included to represent the effect of the input filter. The resistance value was chosen to be equal to 5Ω and the voltage variations at the input and output of the converter were constrained as

$$v_B < 40V, \Delta v_o < 30V \tag{19}$$

Stability Constraints

The stability constraints for the buck converter are somewhat more complicated than the filter. Like the filter, the buck converter must satisfy external stability constraints, so that the entire system in Figure 1 is stable. In addition, because of the presence of the internal control loop, the converter must be internally stable.

Internal Stability Constraints: The design of the feedback controller for the buck converter (Figure 12) must guarantee stability and robustness of the closed loop system in the presence of disturbances in the load current and source voltage. These stability constraints are defined as bounds on the gain margin, g_m, and phase margin, ϕ_m of the closed loop. From classical control theory[10], positive values of phase margin and gain margin are necessary conditions for stability. In order to guarantee sufficient robustness of the closed loop, lower bounds are imposed on these values:

$$\phi_m > 60^o \qquad (20)$$
$$g_m > 3\,\text{dB}$$

These values are widely used in the design of switching converters.

External Stability Constraints: External stability constraints are used to guarantee stability of the interconnected system after adding the input filter. As for the input filter, they are defined using the impedance ratio criterion with the input and output impedances appropriately defined. An upper bound is imposed on the maximum magnitude of the output impedance, Z_{o_max}, and a lower bound on the minimum magnitude of the input impedance, Z_{i_min}, of the closed loop converter, Equation 21.

$$Z_{i\_min} = \min_{\omega}\left(\left|Z_{iB}(j\omega)\right|\right) > 30\,\text{dB} \qquad (21)$$
$$Z_{o\_max} = \max_{\omega}\left(\left|Z_{oB}(j\omega)\right|\right) < 20\,\text{dB}$$

The first of these two constraints ensures that there is at least a 15 dB separation between the output impedance of the filter, which was set to 15dB in Equation 7, and the input impedance of the converter.

Physical Constraints

In addition to the physical constraints, which guarantee physically meaningful dimensions for the core and winding of the inductors, constraints are also imposed to limit the switching ripple in the inductor currents and the capacitor voltages. Although the average model for the buck converter is used for the analysis, expressions for switching ripple in terms of average quantities are readily available.

Inductor Current Ripple: It is generally required that the peak-to-peak inductor current ripple be less than 10% of the nominal inductor current. From Figure 11, the inductor current ripple can be obtained as

$$\Delta I_L = \frac{(1-D)}{f_s}\frac{V_o}{L} \tag{22}$$

The constraint imposing a lower bound on the inductance based on the switching ripple is then determined as follows

$$\Delta I_L < 0.1 I_{L(nom)} \Rightarrow L > 10\left(\frac{V_o^2}{P_o}\right)\left(\frac{1-D}{f_s}\right) \tag{23}$$

$$\text{where, } I_{L(nom)} = \frac{P_o}{V_o}$$

Output Voltage Ripple: The ripple in the output voltage is generally limited to be less than 1% of the average value. The output voltage ripple is the sum of two components, (i) Capacitor voltage ripple and (ii) Ripple due to drop across the resistance R_C. It is assumed that the capacitor absorbs the ripple component of the inductor current. The peak-to-peak output voltage ripple constraint is derived as follows:

$$\Delta V_o = \frac{1}{8C}\frac{\Delta I_L}{f_s} + \Delta I_L R_C \tag{24}$$

Substituting for the inductor current ripple from Equation 22, the output voltage ripple constraint can be determined as follows

$$\Delta V_o = \frac{1}{8LC}\frac{(1-D)}{f_s}V_o + \frac{(1-D)}{Lf_s}V_o R_C = \frac{1}{LC}\frac{(1-D)}{f_s^2}V_o\left(\frac{1}{8} + \tau f_s\right) \tag{25}$$

$$\Delta V_o < 0.01 V_o \Rightarrow LC > 100.\left(\frac{1-D}{f_s^2}\right)\left(\frac{1}{8} + \tau f_s\right),$$

where τ, ESR time constant = $R_c C = 30\ \mu s$.

Objective Function

The objective function is the weight of the converter, which is calculated according to Equation 11 as the sum of the weights of the inductors and the capacitors. The controller is not assumed to contribute significantly to the weight of the converter and hence is neglected in the determination of the weight.

Optimization Results

As was the case for the input filter problem, the VisualDOC optimization software [8] using the Modified Method of Feasible Directions algorithm [9] were used to obtain an optimized design. The transient peak voltage constraint was enforced by imposing an upper bound constraint on the maximum output voltage obtained from a time domain simulation of the filter response. Constraint derivatives were computed using finite differences. Converged optimal designs were obtained in approximately 300 function evaluations (a single function evaluation includes both a

time domain simulation and frequency domain computations). The optimizations were achieved in approximately 20 minutes on a 500 MHz Pentium III PC. The optimal design for the buck converter was insensitive to the initial design.

In order to assess the validity of the results obtained from the optimizer, the optimal designs where compared to a three-phase buck converter for a telecommunications application [5]. This hardware design, developed without the use of the optimizer, is referred to as the nominal design.

The nominal and optimal designs of the buck converter along with the corresponding objective functions are presented in Table 8. .

Table 8. Optimization Results for Buck Converter

Variable	Nominal value	Optimal value
n	55	55.55
A_{cp}	1.1×10^{-5} m^2	1.05×10^{-5} m^2
C_w	1.65×10^{-2} m	1.626×10^{-2} m
W_w	2.5×10^{-2} m	2.28×10^{-2} m
l_g	3.9×10^{-3} m	3.66×10^{-3} m
L	**400 μH**	**419.75 μH**
C	82 μH	46. 88 μF
h_o	1	0.881
ω_z	100 rad/sec	420.14 rad/sec
ω_p	40000 rad/sec	54983 rad/sec
h_{ip}	1	0.998
h_{ii}	100	100
f_s	100kHz	100 kHz
Weight	1.5637 kg	**1.5072 kg**

The nominal and optimal values of inductance obtained from the physical parameters are also listed in Table 8. Response variables of interest for the optimized buck converter are given in Table 9. Response variables at their upper or lower bounds are listed in bold face type. The active constraints for the optimized converter design were the physical constraints on the design of the inductor and the constraint on the input voltage variation to the transient load disturbance. Note that the nominal design violates the constraint on the inductor current ripple.

Table 9. Response quantities for nominal and optimal designs

Response variable	Nominal	Optimal
Inductor current ripple	1.574 A*	1.5A
Capacitor voltage ripple	0.6V	1V
Phase margin	72.5°	69.54°
Gain margin	58.67 dB	37.13 dB
Minimum input	33.72 dB	33.69 dB
Maximum output	0.02 dB	1.25 dB
Audiosusceptibility	-57.24 dB	-55.99 dB
Peak output voltage	19.85 V	22.61 V
Peak input voltage	37.38 V	38.85 V

* Violated constraint

The optimized converter design is not significantly lighter than the nominal design, but it was obtained in a shorter period of time and with a minimal amount of effort compared to the standard manual design procedures.

OPTIMIZATION OF SAMPLE SYSTEM

The optimization procedure for the design of the sample system (combined filter/converter) is presented in this section. The design variables are those of the input filter and the converter as shown in Tables 3 and 7. The constraints on the optimization of the interconnected system are obtained from those of the designs of each of the individual systems with some modifications to account for interactions between the input filter and the converter. The constraints that need to be modified are those that are defined at the interface between the input filter and the converter.

1. Due to the interconnection of the filter and the converter, fixed numbers on the output impedance of the filter and the input impedance of the converter may not be appropriate to imposed as was the case when they were designed independently. Since a sufficient condition for stability is to ensure a minimum separation between the two impedances, the two constraints on the input impedance of the converter, Z_{iB} and the output impedance of the filter, Z_{oF}, are replaced by a single constraint that imposes a lower bound on the difference between the two as shown in Figure 16a.

2. The constraint on the transient excursions on the output voltage of the input filter and the input voltage of the converter are replaced by a single constraint on the maximum excursion of the interface voltage v_B, as shown in Figure 16b.

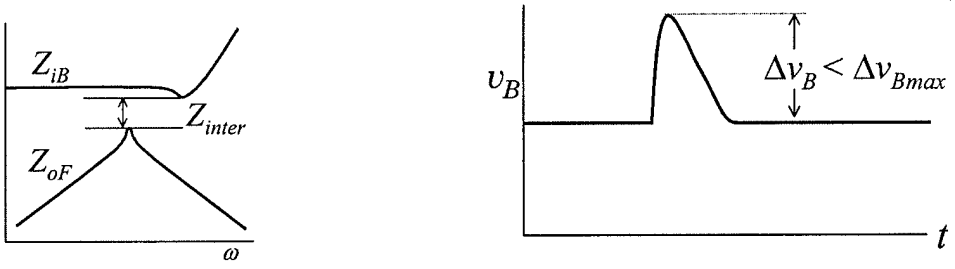

(a) (b)

Figure 16. Interaction constraints on the sample system design Impedance separation (b) Interface voltage variation

The interaction constraints used for the current example are given below:

$$\min_{\omega}\left(\left|Z_{iB}(j\omega)\right|\right) - \max_{\omega}\left(\left|Z_{oF}(j\omega)\right|\right) > 15\,\text{dB} \tag{26}$$

$$\Delta v_B < 20V$$

The 15-dB separation used in the first constraint is consistent with the constraints used for the individually optimized designs (Equations 10 and 21) presented earlier. All other constraints are directly carried over from the optimization formulations of the input filter and the buck converter. The objective function is the total weight of the input filter and converter.

Optimization Results

Converged optimal designs were obtained in approximately 1400 function evaluations, where a single function evaluation again includes both a time domain simulation and frequency domain computations. The optimizations were achieved in approximately 90 minutes on a 500 MHz Pentium III PC. The optimal design was generally insensitive to the initial design, although several local minima were encountered.

The results of the optimization of the sample system are given in Table 10, and important responses are listed in Table 11. The active constraints for the filter in this optimization run were all the physical constraints on the design of the inductors, the lower bound constraint on the input impedance, the upper bound stopband constraint, and the upper bound constraint on the passband. The active constraints on the converter were the physical constraints on the inductor design and the upper bound on the voltage variation at the output due to a load disturbance.

The filter design obtained from the combined problem is lighter than that obtained from the individual optimization. The converter design obtained for the combined optimization problem is almost identical to that obtained independently. Differences in the combined designs and the independently obtained designs arise because the interconnection of two subsystems creates a feedback loop where a change in the source subsystem causes a change in the load subsystem and vice versa. When the optimization was performed on the integrated sample system as a whole, the optimizer was able to take advantage of the interaction between the filter and converter and reduce the overall system weight. The nature of the interaction between the filter and the converter are explained in the following.

Table 10. Comparison of Optimization Results

Variables		Nomimal	Individual Optimization	Integrated Optimization
FILTER	n_1	29.53	19.94	20.01
	A_{cp1}	0.630×10^{-5} m^2	0.530×10^{-5} m^2	0.521×10^{-5} m^2
	C_{w1}	0.751×10^{-2} m	0.484×10^{-2} m	0.480×10^{-2} m
	W_{w1}	0.682×10^{-2} m	1.017×10^{-2} m	1.014×10^{-2} m
	l_{g1}	1.16×10^{-3} m	0.664×10^{-3} m	0.657×10^{-3} m
	n_2	45.98	42.77	42.81
	A_{cp2}	0.448×10^{-5} m^2	0.382×10^{-5} m^2	0.370×10^{-5} m^2
	C_{w2}	0.985×10^{-2} m	0.939×10^{-2} m	0.914×10^{-2} m
	W_{w2}	1.33×10^{-2} m	1.244×10^{-2} m	1.230×10^{-2} m
	l_{g2}	1.29×10^{-3} m	1.03×10^{-3} m	1.017×10^{-3} m
	n_d	16.06	7.79	7.78
	A_{cpd}	0.349×10^{-5} m^2	0.359×10^{-5} m^2	0.356×10^{-5} m^2
	C_{wd}	0.396×10^{-2} m	0.585×10^{-2} m	0.576×10^{-2} m
	W_{wd}	0.978×10^{-2} m	0.564×10^{-2} m	0.561×10^{-2} m
	l_{gd}	0.355×10^{-3} m	0.176×10^{-3} m	0.172×10^{-3} m
	C_1	5 μF	7.19 μF	7.21 μF
	C_2	18.8 μF	27.70 μF	27.86 μF
	R_d	3 Ω	2.23 Ω	2.27 Ω
WEIGHT		**0.5279 kg**	**0.3692 kg**	**0.3495 kg**
	n	55	55.55	55.55
	A_{cp}	1.1×10^{-5} m^2	1.05×10^{-5} m^2	1.05×10^{-5} m^2

C	C_w	1.65 x 10^{-2} m	1.626 x 10^{-2} m	1.63 x 10^{-2} m
O	W_w	2.5 x 10^{-2} m	2.28 x 10^{-2} m	2.28 x 10^{-2} m
N	l_g	3.9 x 10^{-3} m	3.66 x 10^{-3} m	3.67 x 10^{-3} m
V	C	82 µF	46. 88 µF	46.904 µF
E	h_o	1	0.881	0.880
R	ω_z	100 rad/sec	420.14 rad/sec	420.12 rad/sec
T	ω_p	40000 rad/sec	54983 rad/sec	54998.2 rad/sec
E	h_{ip}	1	0.998	0.998
R	h_{ii}	100	100	100
	f_s	100 kHz	100 kHz	100 kHz
WEIGHT		**1.5637 kg**	**1.5072 kg**	**1.5072 kg**

Table 11. Response quantities of Integrated Optimization

Response Quantity		Value
INPUT FILTER	Minimum input impedance	**3.00 dB**
	Maximum output impedance	9.3382 dB*
	Passband maximum	3.36 dB
	Passband minimum	4.87 x 10^{-6} dB
	Stopband maximum	-60 dB
BUCK CONVERTER	Phase margin	69.57°
	Gain Margin	37.18 dB
	Minimum input impedance	33.72 dB*
	Maximum output impedance	1.25 dB
	Audiosusceptibility	-55.98 dB
	Peak output voltage	22.59 V
INTERFACE QUANTITIES	Impedance Difference	24.378 dB
	Peak interface voltage	11.81 V

* These responses were not constrained while performing the integrated optimization. They are shown here for the sake of completeness.

When the input filter is optimized individually, the load disturbance was represented by a pulse load similar to that at the output of the converter except that it was scaled by its duty cycle. When the converter and the filter are optimized together, the load disturbance at the output of the filter (and hence, at the input of the converter) is filtered by the presence of the converter. Hence, the transient peak currents flowing into the inductors of the filter are lesser than those that were present when the filter was optimized individually. This is illustrated in Figure 17 and where the transient responses of the filter inductor current i_{L1}, with and without the buck converter are shown.

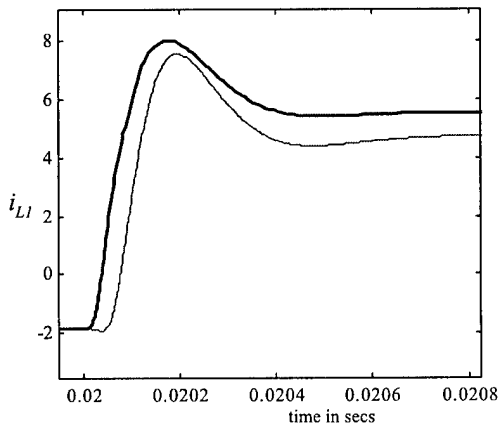

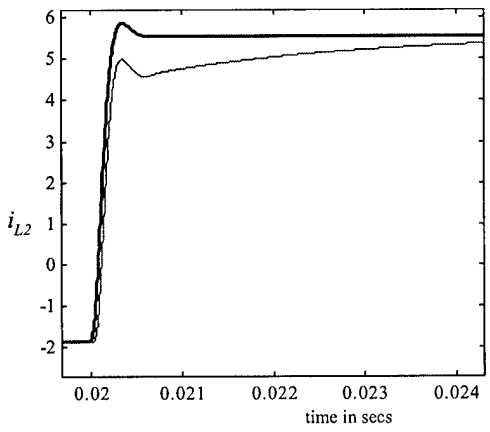

(a) (b)

Figure 17. (a) Filter Inductor current i_{L1} and (b) Filter Inductor Current i_{L2} with (--) and without (-) buck converter

Since, the peak currents flowing into the filter inductors are lower when the converter is taken into account, smaller inductors can be used. This results in a lower weight filter. Simulation results of the sample system with the converter design obtained from the individual and integrated optimizations are shown in Figure 18. It can be seen from Figure 18 that the output voltage variation of the buck converter in the optimized sample system is higher than that of the individually optimized converter. A similar observation can be made from Figures 17a and 17b, where the filter inductor currents are shown. The optimizer increases the capacitance slightly (Table 10) at the output of the buck converter to allow a larger voltage variation. This results in a larger portion of the transient current to flow into the output capacitance of the buck converter than propagate to the filter. This enables the filter weight to be significantly decreased.

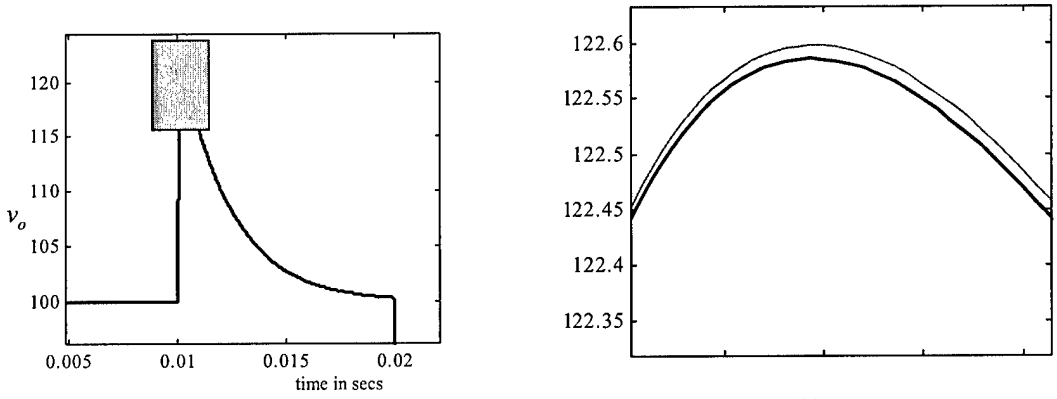

(a) (b)

Figure 18. (a) Converter output voltage in sample system with individually optimized converter design (-) and converter design obtained from optimized sample system (--) (b) Expanded view of shaded area in (a)

The optimizer was, hence, able to take advantage of the system interactions and the more accurate representations of the load disturbances and voltage variations to arrive at an improved (lower weight) design for the combined filter/converter sample system.

The next step in the overall research project is to add additional power system components to the overall optimization problem. As additional components are added, the number of design variables and constraints in the optimization problem will grow accordingly. It is anticipated that the computational expense of the system design problem will eventually become prohibitively large. In this case, an alternative design methodology will be required. It is envisioned that a bi-level global/local design procedure will enable the complete power distribution system to be designed without neglecting important subsystem interactions. Preliminary work on the development of an appropriate global/local methodology for the power distribution system has begun and will be reported in future papers.

CONCLUSIONS

A mathematical optimization problem was formulated for the design of two subsystems of an aircraft power distribution system. A simple interconnected system consisting of an input filter and a regulated DC-DC buck converter was used as a sample system to demonstrate the optimization methodology. It was shown that designing the sample system as a whole resulted in a lesser weight because the optimizer was able to account for the interactions between the interconnected subsystems. The use of optimization methodologies allows designers with a minimum of power electronics design experience to obtain minimum weight designs in a much shorter design cycle time than is required using traditional design techniques.

ACKNOWLEDGEMENTS

The research reported in this paper is supported by the AFOSR under grant numbers F49620-97-1-0254 and F49620-99-1-0104 and made use of ERC Shared Facilities supported by the National Science Foundation under Award Number EEC-9731677.

REFERENCES

1. Fen Chen, et al., "Multi-objective design optimization technique for switching regulators using mixed-discrete programming", *Proceedings of the 20th Annual IEEE Power Electronics Specialists Conference*, June 1989, pp. 526-533.
2. Ridley R. B., et al., "Application of nonlinear design optimization for power converter components", *IEEE Transactions on Power Electronics*, vol. 5. no. 1., January 1990, pp. 29-39.
3. Kragh H, et al., "An advanced tool for Optimized Design of power electronic circuits", *Conference Record of the 1998 IEEE Industry Applications Conference*, vol. 1, October 1998, pp. 991-998.
4. Hopkins D. C., et al., "A mathematical approach to minimize the total mass of a space based power system by using multivariate non-linear optimization", *Proceedings of the 29th Intersociety Energy Conversion Engineering Conference*, vol. 1, August 1994, pp. 185-189.
5. Wang, K, Chandrasekaran, S., and Cuadros, C., et al., "Quasi-Single Stage Three phase ZVZCS PWM Buck Rectifier", Virginia Power Electronics Center-Project Report submitted to Ericsson Components, Sweden, March 1999.
6. J. G. Kassakian, M. F. Schlecht, G. C. Verghese, "Principles of Power Electronics," Addison-Wesley, 1991.
7. Middlebrook, R. D., "Input Filter Considerations in Design and Application of Switching Regulators," *IEEE Industry Application Society Annual Meeting*, October 11-14, 1976, Chicago, Il.
8. Vanderplaats, G.N., *Numerical Optimization Techniques for Engineering Design: With Applications*, Vanderplaats R&D Inc., Colorado Springs, CO, 1988.
9. Haftka, R.T., and Gürdal, Z., *Elements of Structural Optimization, Third Revised and Expanded Edition*, Kluwer Academic Publishers, Dordrecht, 1992, pp. 182-186.
10. Ogata. K, "Modern Control Engineering", Prentice Hall, Eastern Economy Edition, 1986.